ISSN 1067-8212, Russian Journal of Non-Ferrous Metals, 2018, Vol. 59, No. 5, pp. 471–475. © Allerton Press, Inc., 2018.
Original Russian Text © V.V. Stakhanov, A.A. Redkin, Yu.P. Zaikov, A.E. Galashev, 2018, published in Izvestiya Vysshikh Uchebnykh Zavedenii, Tsvetnaya Metallurgiya, 2018, No. 4, pp. 24–30.

METALLURGY
OF NONFERROUS METALS

Influence of Electrolyte Overheating and Composition on the Sideledge of an Aluminum Bath

V. V. Stakhanov[a, *], A. A. Redkin[a, **], Yu. P. Zaikov[a, b, *], and A. E. Galashev[a, ****]**

[a] *Institute of High-Temperature Electrochemistry, Ural Branch, Russian Academy of Sciences, Yekaterinburg, 620219 Russia*

[b] *Ural Federal University, Yekaterinburg, 620002 Russia*

**e-mail: slavastahanov@mail.ru*

***e-mail: a.redkin@ihte.uran.ru*

****e-mail: dir@ihte.uran.ru*

*****e-mail: alexander-galashev@yandex.ru*

Received December 21, 2017; in final form, April 19, 2018; accepted for publication April 27, 2017

Abstract—The effect of the electrolyte chemical composition and overheating on the size of a sideledge formed in an aluminum-smelting bath is investigated theoretically. Three electrolyte compositions are chosen: sodium cryolite with the cryolite ratio (CR) = 2.7, cryolite (CR) = 2.7 + 5 wt % CaF_2, and cryolite (CR) = 2.7 + 5 wt % CaF_2 + 5 wt % Al_2O_3. The electrolyte liquidus overheating temperatures are 5, 10, 15 and 20°C. The calculations are performed using the finite-element method. A simplified design of an aluminum cell with a prebaked anode is used. To calculate the temperature field, a mathematical model in the Boussinesq approximation is used. The model contains the Navier–Stokes equation, the thermal conductivity equation, and the incompressibility equation. The key role of electrolyte overheating on the sideledge formation is established. The resulting sideledge profile depends on the heat transfer coefficients and thermal properties of materials. The smallest sideledge thickness with the same electrolyte overheating is observed in cryolite with CR = 2.7, 5 wt % CaF_2, and 5% by weight of Al_2O_3, and formed sideledge profiles for cryolite with KO = 2.7 and cryolite with KO = 2.7 and 5 wt % CaF_2 almost coincide. The thickness of the sideledge formed with overheating of 5 K is from 7 cm or more, and the difference in temperature between the sideledge touching the electrolyte and airborne block wall is 20–25 K. Almost complete sideledge disappearance occurs when the electrolyte liquidus is overheated by 20 K.

Keywords: aluminum, sideledge, temperature field, modeling, finite element method, electrolyzer, overheating

DOI: 10.3103/S1067821218050188

INTRODUCTION

The main tendency in the development of aluminum industry in recent years is an increase in the current load of electrolysis baths. Fifteen years ago, apparatuses with a current of 80 kA were considered high-amperage [1]; on the contrary, high-amperage installations are those with a current load higher than 400 kA [2, 3]. The rise in power of electrolyzers makes elevated demands to construction materials and, in addition, leads to an increase in heat flows, which makes heat equilibrium more unstable. This is the cause of the formation instability of the protective sideledge and shortening of the bath service life.

The main parameter determining the sideledge sizes and structure is electrolyte overheating, i.e., the excess of the electrolyzer working temperature over the melt liquidus temperature [4, 5]. This parameter should be held constant; however, any variations in the salt-bath composition will cause a variation in the liquidus temperature, which will affect the overheating magnitude. Alumina and calcium fluoride additives substantially affect the melt liquidus temperature. The variation in their content also affects other properties such as heat and electrical conductivity, which also affects the temperature distribution in the electrolyzer volume. The determination of the sideledge profile in actual conditions for various electrolyte compositions requires numerous repetitions of experimental investigations and, consequently, the time necessary for this purpose, which is impossible in practice under conditions of an industrial electrolyzer in operation. Therefore, modeling formation processes of the protective layer of the solidified electrolyte on the sidewall of the aluminum electrolyzer unit becomes topical.

The electrolyzer temperature field can be modeled using the finite element method (FEM) [6–8]. The introduction of the "finite element" notion makes it possible to overcome the problem of an infinite amount of connection points of the solid body by its division into finite elements (of the computable

amount) interacting between each other only in connection points.

This method started to be applied to model the processes occurring in an aluminum electrolyzer as far back as 30 years ago [9]. Initially these were partial problems which concerned separate electrolyzer constructions, but models for the apparatuses in general started to be developed with time. The FEM is most often used to model the temperature distribution in the electrolyzer volume depending on the influence of various factors. Analyzing temperature fields can be also fulfilled using other methods. In particular, researchers at Auckland University developed their own program for calculating this characteristic of the aluminum electrolyzer based on the solution by the FEM [10, 11].

The task of this study was to investigate the influence of the electrolyte composition and its overheating on the sideledge formation. The calculation of thermal and electric fields in the electrolyte was performed with the help of the FEM implemented in the ANSYS v.17.2 software. We used a simplified design of the aluminum electrolyzer with prebaked anodes. Its application simplifies calculations without varying the character of the influence of the electrolyte composition and overheating on the sideledge parameters. We further plan to perform calculations for designs similar to those used in industry.

COMPUTATIONAL MODEL

To calculate the electrolyzer temperature and electric fields which affect the sideledge profile, the equations presented below are solved.

Temperature Field

To describe the convection in liquids and gases, heat convection equations in the Boussinesq approximation are applied. The model includes of the equations of Navier–Stokes, heat conductivity, and incompressibility. Chemical processes occurring in the electrolyte volume are indirectly taken into account in parameters specified in the mathematical model.

To solve the problems associated with finding the temperature field, we need the differential heat conductivity equation, which describes the dependence between temperature, time, and unit volume coordinates:

$$\rho c \frac{\partial T}{\partial t} = \lambda\left(\frac{\partial^2 T}{\partial x^2} + \frac{\partial^2 T}{\partial y^2} + \frac{\partial^2 T}{\partial z^2}\right) + Q, \qquad (1)$$

where λ is the heat conductivity coefficient, W/(m K); c is heat capacity, J/(kg K); ρ is the material density, kg/m^3; and Q is the internal heat liberation, W/m^3, which is associated with the Joule heat liberation during the electric current passage.

The Navier–Stokes equation has the form

$$\rho_0\left(\frac{\partial v}{\partial t} + (v\cdot\nabla)v\right) = -\nabla p + \eta\Delta v + \rho(T)g, \qquad (2)$$

where v is the liquid flow velocity, m/s; p is the pressure, Pa; η is the dynamic viscosity, Pa s; and $g = 9.81$ m/s^2 is the acceleration of gravity.

To describe the temperature dependence of density, the linear approximation is applied:

$$\rho(T) = \rho_0(1 - \beta\theta), \qquad (3)$$

where ρ_0 is the liquid density at equilibrium temperature T_0, kg/m^3; β is the coefficient of volumetric expansion, K^{-1}; and $\theta = T - T_0$ is the deviation of temperature from the equilibrium state, K.

The incompressibility equation is presented in the form

$$\mathrm{div}v = 0. \qquad (4)$$

Continuous heat fluxes in the electrolyzer volume caused by heat conduction, convection, and radiation affect the sideledge formation. Consequently, to solve the stated problem, all three types of heat transfer should be taken into account.

The variation in the heat flux density due to heat conduction is determined by the Fourier law:

$$\mathbf{q} = -\lambda\left(\frac{\partial T}{\partial x}\mathbf{i} + \frac{\partial T}{\partial y}\mathbf{j} + \frac{\partial T}{\partial z}\mathbf{k}\right), \qquad (5)$$

where **i, j,** and **k** are unit vectors in the Cartesian coordinate system.

The heat flux density on the boundaries of the electrolyte and wall, electrolyte and sideledge, and outer electrolyzer walls and surrounding air in the case of convective heat conduction is determined according to the Newton–Richman formula:

$$q_k = \alpha_k(t_1 - t_2), \qquad (6)$$

where α_k is the heat emission coefficient at corresponding boundaries, W/(m^2 K); and $(t_1 - t_2)$ is the temperature difference between the wall and medium, K.

The account of the radiation influence on the temperature field is performed based on the temperature dependence of the integral density stated by the Stephan–Boltzmann law:

$$E = \varepsilon c_0 T^4, \qquad (7)$$

where $c_0 = 5.67 \times 10^{-8}$ W/(m^2 K^4) $= 20.41 \times 10^{-8}$ kJ/(m^2 h K^4) is the Stephan–Boltzmann constant and ε is the emissivity factor of the radiating body surface.

To determine the temperature fields, boundary conditions that will be presented below should be used.

Electric Field

The electric field inside any conductor, including an electrolyte, located in the electrolytic cell is characterized by the following set of equations:

$$\begin{cases} \mathrm{div}\mathbf{j} = 0, & (8) \\ \mathbf{j} = \sigma\mathbf{E}, & (9) \\ \mathrm{rot}\mathbf{E} = 0, & (10) \end{cases}$$

where $\mathbf{j}$ is the current density, A/m^2; σ is specific conductivity, $(\Omega\ \mathrm{m})^{-1}$; and $\mathbf{E}$ is the electric field strength, V/m.

Equality (8) is the charge conservation law and represents the generalized form of the first Kirchhoff law in the differential form, Eq. (9) reflects the connection between the electric-field strength and current density, and equality (10) shows that the field of constant currents has an eddy-free character and reflects the second Kirchhoff law in the differential form. Herewith, Eq. (8) turns out equivalent to the equality

$$\mathbf{E} = -\mathrm{grad}\varphi, \quad (11)$$

where φ is the electric field potential, V.

Based on expressions (9) and (11), we can write the differential equation of the Ohm law in the form

$$\mathbf{j} = -\sigma\,\mathrm{grad}\varphi. \quad (12)$$

The solution of problems on the distribution of the electric field potential is in general reduced to the integration of the totality of differential Eqs. (8), (9), and (10) under definite boundary conditions. It follows from formulas (8), (9), and (11) that

$$\mathrm{div}\mathbf{j} = \mathrm{div}\left(\sigma\mathrm{grad}\varphi\right) = 0. \quad (13)$$

The specific electrolyte conductivity (σ) entering Eq. (13) can depend on coordinates of the point under consideration $\sigma(x, y, z)$. The variation in the electrolyte specific conductivity during the current flowing can be as a rule neglected for industrial electrolyzers, systems of the anticorrosion protection of apparatuses, and in many other cases of applying the electrolytic cells—i.e., σ = const. Equation (13) transforms into the Laplace differential equation in this case:

$$\frac{\partial^2\varphi}{\partial x^2} + \frac{\partial^2\varphi}{\partial y^2} + \frac{\partial^2\varphi}{\partial z^2} = 0. \quad (14)$$

The determination of the electric current is in most cases reduced to the solution of this equation at corresponding boundary conditions. When deriving it in the form of the expression for potential $\varphi(x, y, z)$, we can also easily calculate other parameters of the electrolyzer electric field. For example, to determine the components along coordinate axes of the current density vector, we can use relationship (12):

$$j_x = -\sigma\frac{\partial\varphi}{\partial x}, \quad j_y = -\sigma\frac{\partial\varphi}{\partial y}, \quad j_z = -\sigma\frac{\partial\varphi}{\partial z}. \quad (15)$$

In this study, we accepted the following boundary conditions corresponding to average values for industrial electrolyzers [15, 16]:

• anode current density $j = 0.85$ A/cm^2;

• convective heat exchange coefficients for various media:

α_k = 12 W/(m^2 K) for aluminum lead (the surrounding medium temperature is 35°C);

α_k = 1000 W/(m^2 K) for the electrolyte medium (the surrounding medium temperature corresponds to the cryolite liquidus temperature with overheating by 5, 10, 15, or 20°C);

α_k = 20 W/(m^2 °C) for a steel case (the surrounding medium temperature is supposed to be equal 35°C).

• the zero potential was specified on the lower cathode surface.

The radiation thermal distribution was determined based on using the reference data on the emissivity (ε) of each material. The data on the properties of construction materials of the electrolyzer necessary for calculations are presented in [17–23].

Calculations were performed for three electrolyte compositions:

(1) cryolite with cryolite ratio (CR) = 2.7;

(2) cryolite with CR = 2.7 + 5 wt % CaF_2;

(3) cryolite with CR = 2.7 + 5 wt % CaF_2 + 5 wt % Al_2O_3.

Properties of electrolytes (the liquidus temperature, density, electrical conductivity, heat conductivity, and dynamic viscosity) were calculated based on the published data [12].

GEOMETRIC MODEL OF THE ALUMINUM ELECTROLYZER

To calculate the sideledge profile, we selected a simplified model of the aluminum electrolyzer with a prebaked anode (Fig. 1). A steel electrolyzer case has outer sizes of 189 × 120 × 268 cm. Aluminum cathode and anode current leads are used in the design. The current lead is connected with the anode with the help of a steel three-phase "spider". The electrolyte with molten aluminum is arranged in a coal bottom, the design of which is simplified in a model. The distance between the cathode and anode is 5 cm and, between the sidewall bordering with the electrolyte and anode, it is 40 cm. The electrolyte boundaries are created by side blocks made of SiC. The space between the outer steel case and bottom is filled by a heat insulation and dry barrier mixture.

The constructed geometric model of the electrolyzer is divided into finite elements (Fig. 2), the maximal size of which is 2 cm and the minimal one is 0.05 cm. These sizes depend on the degree of varying the parameters; therefore, the finite element size in the electrolyte bulk is smallest.

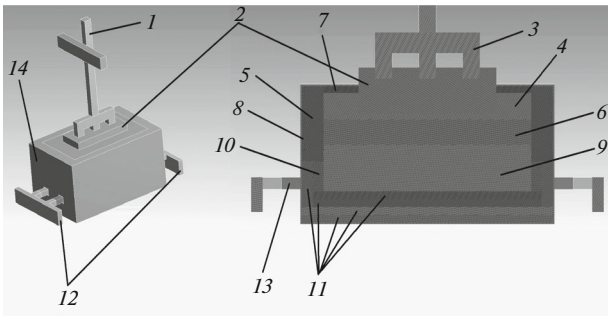

Fig. 1. Geometric model of the aluminum electrolyzer. (*1*) Current lead (aluminum), (*2*) anode, (*3*) spider (steel), (*4*) electrolyte, (*5*) side block (SiC), (*6*) liquid aluminum, (*7*) alumina, (*8*) dry barrier mixture, (*9*) bottom block (graphite), (*10*) bottom mass, (*11*) heat insulation (thermoinsulating vermiculite, fire-resistant chamotte), (*12*) cathode current leads, (*13*) steel blooms, and (*14*) steel case.

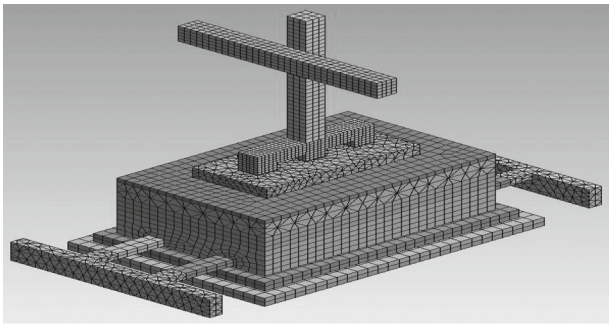

Fig. 2. Geometric model of the aluminum electrolyzer divided into finite elements.

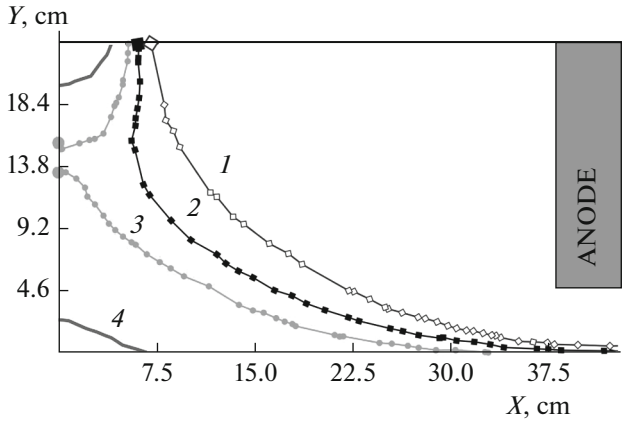

Fig. 3. Sideledge profile at various values of overheating for sample *3* (cryolite + 5 wt % CaF_2 + 5 wt % Al_2O_3). (*1*) Overheating 5, (*2*) 10, (*3*) 15, and (*4*) 20 K.

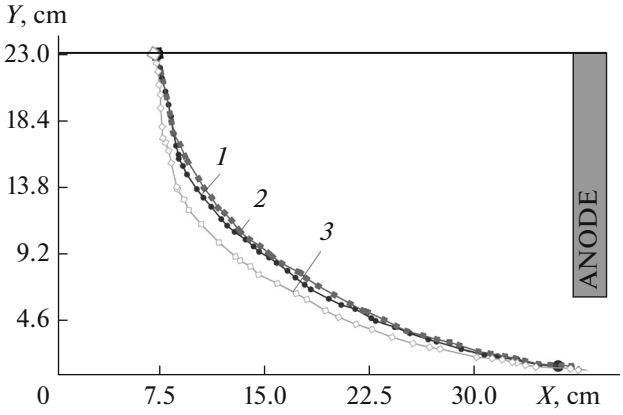

Fig. 4. Variation in the sideledge profile depending on the electrolyte composition with 5-K overheating. (1) Cryolite (CR = 2.7), (2) cryolite + 5 wt % CaF_2, and (3) cryolite + 5 wt % CaF_2 + 5 wt % Al_2O_3.

RESULTS OF CALCULATIONS

The results of calculating the sideledge profile at various values of overheating and electrolyte compositions are presented in Figs. 3 and 4 (the distance from the side block to the anode is counted along *X* axis, and the electrolyte height is counted along *Y* axis).

It is seen from Fig. 3 that overheating most strongly affects the sideledge formation. The maximal sideledge thickness is observed with 5-K overheating, while the complete sideledge disappearance is possible with 20-K overheating. The influence of the electrolyte composition with invariable 5-K overheating is rather limited (Fig. 4). They aspire to hold just this its value when producing aluminum.

The results of calculations point to the fact that the appearance of the smallest sideledge thickness should be expected for alumina-containing cryolite, other conditions being equal. This is explained by the fact that the presence of alumina in the melt substantially decreases the coefficient of heat conductivity of the electrolyte, which leads to a small decrease in the sideledge volume. Other parameters affect the sideledge indirectly through the melt overheating, which can occur for various reasons and first and foremost—due to an increase in the electrolyzer power.

Model calculations of various researchers show the direct correlation between overheating and sideledge thickness; however, no agreement is attained in numerical evaluations. According to the authors of [7], the variation in overheating from 9 to 15 K insignificantly affects the sideledge thickness, while the results presented in [8] forecast the sideledge disappearance with 15-K overheating. Herewith, the maximal sideledge thickness with the 5-K overheating is from 7 cm, while the temperature difference between the sideledge touching the electrolyte and side block wall is 20–25 K.

Our calculations also show the sideledge disappearance at 20-K overheating. It is highly likely that such divergences are associated with the use of various calculation parameters, first and foremost, heat transfer coefficients, which considerably differ by various authors [13, 14].

CONCLUSIONS

Model calculations of the sideledge profile for various electrolyte compositions and for various values of melt overheating are performed by the finite element method. It is revealed that overheating exerts a decisive influence on the sideledge coating shape and sizes. Its thickness for the 5-K overheating is from 7 cm and larger, while it almost disappears with 20-K overheating.

The electrolyte properties with fixed overheating insignificantly affect the sideledge profile. However, the presence of alumina in electrolyte somewhat decreases its thickness, because Al_2O_3 lowers the coefficient of heat conductivity of the melt. The variation in the electrolyte composition indirectly affects the formed sideledge profile because this leads to a variation in the liquidus temperature and, consequently, the magnitude of overheating.

The proposed mathematical model can be used to calculate the more complex, from the viewpoint of this process, industrial electrolyzer designs having other sizes and a bath shape.

ACKNOWLEDGMENTS

This study was supported by the Ministry of Education and Science of the Russian Federation, agreement no. 14.607.21.0146; the unique agreement identifier is RFMEFI60716X0146.

REFERENCES

1. Capitance, W. and Schmidt-Hatting, W., Magnetic fields in high amperage aluminum reduction cells, *JOM*, 1965, vol. 17, no. 3, pp. 271–275.
2. Zhou, J. and Dupuis, M., *In-depth analysis of lining designs for several 420 kA electrolytic cells*, *Light Met,* 2015, pp. 685–690.
3. Welch, B.J., Hyland, M.M., and James, B.J., Future materials requirements for the high-energy-intensity production of aluminum, *JOM*, 2001, vol. 53, no. 2, pp. 13–18.
4. Kvande, H., Bath chemistry and aluminum cell performance: facts, fictions, and doubts, *JOM*, 1994, vol. 46, no. 11, pp. 22–28.
5. Haupin, W., The influence of bath additives on Hall-Heroult bath properties, *JOM*, 1991, vol. 43, no. 11, pp. 28–34.
6. Dupuis, M., *Computation of aluminum reduction cell energy balance using ANSYS® Finite element models*, *TMS Light Met.*, 1998, pp. 409–417.
7. Beier, S., Chen, J., Fortin, H., and Fafard, M., *FEM analysis of the anode connection in aluminum reduction cell*, *Light Met.*, 2011, pp. 979–984.
8. Wei, L., Jie, L., Yan-qing, L., and Ye-xiang, L., 2D Finite element analysis of thermal balance for drained aluminum reduction cells, *J. Centr. South Univ. Technol.*, 2007, vol. 14, no. 6, pp. 783–787.
9. Dupius, M., Using ANSYS to model aluminum reduction cell since 1984 and beyond, in *Proc. ANSYS Reg. Conf.*, Toronto, 2002.
10. Taylor, M., Etzion, R., Lavoie, P., and Tan, J.N., Energy balance regulation and flexible production: A new frontier for aluminum smelting, *Metall. Mater. Trans. E*, 2014, vol. 1, no. 4, pp. 292–302.
11. Lavoie, P., Namboothiri, S., Dorreen, M., Chen, J., Zeigler, D., and Taylor, M., *Increasing the power modulation window of aluminium smelter pots with shell heat exchanger technology*, *Light Met.*, 2011, pp. 369–374.
12. Thonstad, J., Fellner, P., Haarberg, G.M., Hives, J., Kvande, H., and Sterten, A., *Aluminium Electrolysis: Fundamentals of the Hall-Heroult Process*, Dusseldorf: Aluminium-Verlag Market. Kommun., 2001, 3rd ed.
13. Solheim, A., *Some aspects of heat transfer between bath and sideledge in aluminium reduction cells*, *Light Met.*, 2011, pp. 381–386.
14. Taylor, P. and Welch, B., Melt/freeze heat transfer measurements in cryolite-based electrolytes, *Metall. Trans. B*, 1987, vol. 18, no. 2, pp. 391–398.
15. Borisoglebskii, Yu.B., Galevskii, G.V., Kulagin, N.M., Mintsis, M.Ya., and Sirazutdinov, G.A., *Metallurgiya aluminiya: Uchebnoe posobie* (Aluminum Metallurgy: Textbook), Novosibirsk: Nauka, 1999.
16. Arkhipov, G.V., Pingin, V.V., Tretyakov, Y.A., and Polyakov, P.V., *Simulation of cell thermoelectric field with consideration of electrochemical processes*, *Light Met.*, 2007, pp. 327–331.
17. Balkevich, V.L., *Tehnicheskaya keramika: Uchebnik dlya vysshykh uchebnykh zavedenii* (Technical Ceramics: Textbook for Higher Schools), Moscow: Stroiizdat, 1984.
18. *ASM Metals Handbook. Vol. 1: Properties and Selection: Irons, Steels, and High-Performance Alloys*, ASM, 1990, 10th ed.
19. Desai, P.D., Chu, T.K., James, H.M., and Ho, C.Y., Electrical resistivity of selected elements, *J. Phys. Chem. Ref. Data*, 1984, vol. 13, no. 4, pp. 1069–1096.
20. Shinno, H., Kitajima, M., and Okada, M., Thermal stress analysis of high heat flux materials, *J. Nucl. Mater.*, 1988, vols. 155–157, pp. 290–294.
21. Giordanengo, B., Benazzi, N., Vinckel, J., Gasser, J.G., and Roubi, L., Thermal conductivity of liquid metals and metallic alloys, *J. Non-Cryst. Solids*, 2000, vols. 250–252, pp. 377–383.
22. Gale, W.F. and Totemeier, T.C., *Smithells Metals Reference Book*, Amsterdam: Elsevier, 1988.
23. Iida, T. and Guthrie, R.I.L., *The Physical Properties of Liquid Metals*, Oxford: Clarendon, 1988.

Translated by N. Korovin